Since January 2020 Elsevier has created a COVID-19 resource centre with free information in English and Mandarin on the novel coronavirus COVID-19. The COVID-19 resource centre is hosted on Elsevier Connect, the company's public news and information website.

Journal of Molecular Structure 1220 (2020) 128715

Contents lists available at ScienceDirect

Journal of Molecular Structure

journal homepage: http://www.elsevier.com/locate/molstruc

DFT studies on vibrational and electronic spectra, HOMO–LUMO, MEP, HOMA, NBO and molecular docking analysis of benzyl-3-N-(2,4,5-trimethoxyphenylmethylene)hydrazinecarbodithioate

Mohammad Abdul Mumit [a], Tarun Kumar Pal [a, *], Md Ashraful Alam [a], Md Al-Amin-Al-Azadul Islam [a], Subrata Paul [b], Md Chanmiya Sheikh [c]

[a] Department of Chemistry, Rajshahi University of Engineering & Technology, Rajshahi, 6204, Bangladesh
[b] Department of Pharmacy, Rajshahi University, Rajshahi, 6205, Bangladesh
[c] Faculty of Environmental and Life Science, Okayama University, Okayama, 700-8530, Japan

ARTICLE INFO

Article history:
Received 21 April 2020
Received in revised form
5 June 2020
Accepted 15 June 2020
Available online 20 June 2020

Keywords:
DFT
NBO
HOMA
Molecular docking
ADMET

ABSTRACT

Benzyl-3-N-(2,4,5-trimethoxyphenylmethylene)hydrazinecarbodithioate (compound **1**) is a bidentate and nitrogen-sulfur containing Schiff base, which has been synthesized by the condensation reaction of S-benzylndithiocarbazate and 2,4,5-trimethoxybenzaldehyde. The theoretical calculations of the mentioned compound have been carried out using the more popular density functional theory method, Becke-3-Parameter-Lee-Yang-Parr (B3LYP) in 6-31G+(d,p) basis set. The computational results of the compound were compared with the obtained experimental value. Moreover, the highest occupied molecular orbital, the lowest unoccupied molecular orbital, molecular electrostatic potential, chemical reactivity parameters and natural bond orbital of the optimized structure have been evaluated at the same level of theory. Furthermore, the UV–Vis spectrum of the compound has been carried out for the better understanding of electronic absorption spectra with the help of the time-dependent density functional theory at room temperature. Besides, the molecular docking simulation of the mentioned molecule with target protein was also investigated. In addition, *in silico* studies were performed to predict absorption, distribution, metabolism, excretion and toxicity profiles of the designed compound. The results indicated that the theoretical data have well correlated with the observed values. The narrow frontier orbital gap indicated that the eventual charge transfer interaction occurs within the studied molecule and showed high chemical reactivity. The global reactivity values showed that the compound is soft molecule, electrophilic species and has strong binding ability with biomolecules. The molecular electrostatic potential structure indicated that the negative and positive potential sites are around electronegative atoms and hydrogen atoms of studied compound, respectively. The natural bond orbital data revealed that the compound contains 97.42% Lewis and 2.58% non-Lewis structure. The intra and inter-molecular charge transfers process occur within the studied compound. The studied compound showed more binding energy (−6.0 kcal/mol) with target protein than hydroxychloroquine (−5.6 kcal/mol). The absorption, distribution, metabolism, excretion and toxicity investigation predicted that the compound has good drug like character.

1. Introduction

S-benzyl dithiocarbazates (SBDTC) are nitrogen-sulfur consisting of organic compounds and can easily coordinate with metal ions due to the presence of hard nitrogen and soft sulfur donor atoms [1–5]. S-benzyl dithiocarbazate and its substituted derivatives have been shown significant biological activities [6–13]. Therefore, owing to their versatile coordination character and promising biological properties, a large number of Schiff bases have been synthesized and reported from SBDTC and various aromatic aldehydes or ketones [2,3,6,7]. Dithiocarbazate Schiff bases have been shown cis-trans and trans-cis isomers in solid-state with respect to the N–C and C–S bond. Moreover, Some of these

* Corresponding author.
E-mail addresses: tkpchem@gmail.com, tkpal@chem.ruet.ac.bd (T.K. Pal).

https://doi.org/10.1016/j.molstruc.2020.128715
0022-2860/

dithiocarbazate Schiff bases have interesting applications in the area of electronic engineering as solar cell components, non-linear optical materials [6,7,9,14–18] and of medicinal field as antifungal, antibacterial, anticancer and antioxidant [7,14,19–24]. Recently, most of the researchers are highly interested in computational methods to assist the experimental evidences of chemical species. The theoretical methods play an important role for the investigation of the chemical reaction and several molecular properties of the chemical species. Besides, the theoretical methods are mostly used for the identification of proposed structure of newly synthesized chemical species, due to their high efficiency and accuracy. From this point of view and continuation of our previous research work [7], the current study is an effort to investigate of computational calculation of the mentioned Schiff base in details. However, to the best of our knowledge, no theoretical study of S-benzyl dithiocarbazate Schiff base has been published in the literature so far. Density functional theory (DFT) [25–28] calculation having vibrational frequency is an essential for theoretical studies of organic molecules and related fields. Besides, DFT approach is very important and helpful tool to explore the relationship between geometry and electronic properties of chemical compound [18,28,29] Therefore, we report herein DFT calculations involving vibrational frequency analysis, electronic spectra, highest occupied molecular orbital (HOMO)-lowest unoccupied molecular orbital (LUMO) energy with various chemical reactivity parameters, mulliken population analysis, molecular electrostatic potential, HOMA index, natural population analysis, natural bond orbital (NBO) investigation of the Schiff base, benzyl-3-N-(2,4,5-trimethoxyphenylmethylene)hydrazinecarbodithioate. The theoretically computed infrared, UV–Visible, bond length and bond angle were compared with experimental values. All experimental values have been carried out using pure single crystal compound. In addition, molecular docking of SBDTC Schiff base, azithromycin and hydroxychloroquine with the target protein, coronavirus, 6LU7 was investigated as well as the absorption, distribution, metabolism, excretion and toxicity (ADMET) prediction was also performed to assess the drug-likeness and toxicity profile of the mentioned compound.

2. Method

2.1. Synthesis of NS-Schiff base

The NS-Schiff base, benzyl-3-N-(2,4,5-trimethoxyphenylmethylene)hydrazinecarbodithioate has been synthesized by the method of our previous reports [7,14].

2.2. Computational details

The molecular structure (Fig. 1) was drawn using GaussView 6.0.16 software [30]. The full molecular geometry optimization of the compound was carried out by employing the density functional theory at B3LYP level [31] and 6-31G+(d,p) basis set with the help of Gaussian 09W software package [32]. The optimized structure of the compound **1** (Fig. 1) has been used to calculate the molecular electrostatic potential, highest occupied molecular orbital and lowest unoccupied molecular orbital energy by Gaussian 09W software. The vibrational frequencies were measured at the same level of theory for the optimized geometry and found frequencies were scaled 0.9614 [33,34].The electronic excitations of the optimized neutral compound were also measured using the time-dependent density functional theory in gas phase. For the molecular docking simulation, first of all, the initial 3D structure of the above mentioned compound was drawn in GaussView 6.0.16 software. Then the structure was saved as single file and PDB format via PyMol software [35]. Secondly, the crystal structure of selected protein (PDB code: 6LU7) was collected from the protein data bank server (www.rcsb.org) as PDB format. All water molecules, ions and ligands were removed from the crystal structure of the target protein through PyMol software. In the case of studied compound, OpenBabel of PyRx software [36] was used to minimize and convert the.pdb files to the AutoDock docking format (.pdbqt). While, the receptor protein was minimized and converted the.pdb files to the AutoDock docking format (.pdbqt) in PyRx software for afterward docking. AutoDock Wizard in a virtual screening software, PyRx was used for the molecular docking simulation between studied compound and target receptor. The predicted docking poses of the compound-protein complex were visually investigated using Discovery studio 4.5 software [37].

3. Results and discussion

3.1. Infrared spectra

The FTIR spectra were shown in Fig. 2. The mentioned compound was showed a characteristic band at 3103 cm^{-1} due to thione group [−NH−C(=S)-] [7,14,38] which was theoretically calculated as 3461 cm^{-1}. The aromatic C=C bonds showed at 1608 cm^{-1} [7,39], which was found at 1631 cm^{-1} based on the theoretical spectrum. The most characteristic azomethine group *ν*(C=N) band was observed at 1595 cm^{-1} experimentally [1,19,38,40–44], where theoretical calculation produced this band at 1668 cm^{-1}. The studied compound was appeared a band at 1097 cm^{-1} that attributed to symmetric stretching of ν(C=S) [7,14,38], which were theoretically observed at 1139 cm^{-1} using the B3LYP/6-31G+(d,p) computation method.

3.2. Electronic spectra

The UV–visible absorption spectrum is used to calculate the charge transfer phenomena in organic compounds. The UV-VIS spectrum of the compound **1** was studied within the range 200–800 nm and the electronic spectrum of the compound was done by TD-DFT method as theoretically. The experimental and theoretical spectra are given in Fig. 3. The electronic absorption spectrum of the compound was appeared four medium to instance bands at 241, 289, 316 and 395 nm experimentally. These transitions could be attributed to the $\pi \rightarrow \pi^*$ transition of aromatic, $\pi \rightarrow \pi^*$ transition of azomethine, $n \rightarrow \pi^*$ transition of azomethine and $n \rightarrow \pi^*$ transition of dithiocarbazate moiety, respectively [7]. While, the studied compound was showed only three absorption bands at 320, 387 and 410 nm in DFT obtained spectrum, which may be attributed to $\pi \rightarrow \pi^*$ transition of azomethine, $n \rightarrow \pi^*$ transition of azomethine and $n \rightarrow \pi^*$ transition of dithiocarbazate moiety, respectively. Thus, the results revealed that the DFT determined wavelength is in good agreement to the observed wavelength.

3.3. Crystal structure interpretation

The crystal structure, bond length and bond angle of the compound **1** has been carried out by single crystal X-ray diffraction technique using a single crystal with the dimensions of 0.200 × 0.125 × 0.090 mm [7]. The studied compound crystallizes in monoclinic system with space group $P2_1/c$. The calculated bond length and bond angle for compound **1** were determined with the help of GaussView 6.0.16 software. An ORTEP drawing and optimized structures of the mentioned compound is given in Fig. 1. The selected bond length and bond angle for compound **1** are shown in Table 1, which were compared to the correspondent geometrical

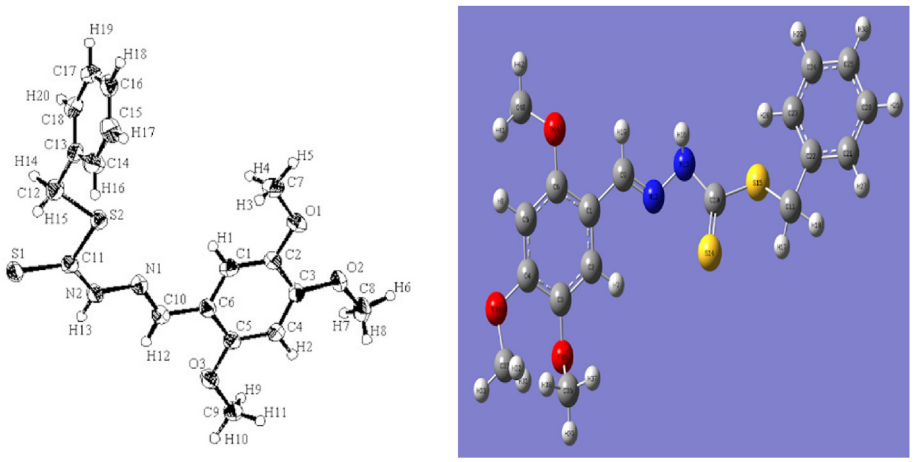

Fig. 1. Crystal (left) and optimized structure (right) with atoms numbering of compound 1.

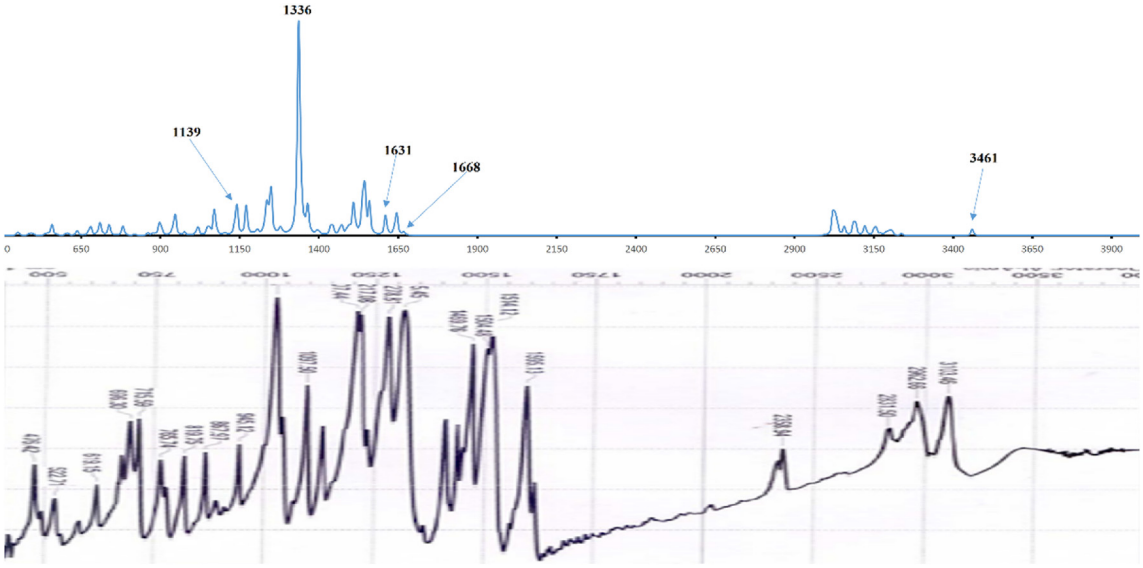

Fig. 2. Theoretical (up) and experimental (down) infrared spectrum of compound 1.

parameters of observed data.

From the graph, a linearity was found between the calculated and experimental data (Figs. 4 and 5). The correlation coefficient (R^2) of bond length and bond angle of the studied compound was found to be 0.9492 and 0.8488, respectively in the case of experimental and calculated data. Thus, it can be concluded that the bond length and bond angle values obtained from DFT method were consistent with the observed data.

The crystal data showed that C10 = N1 bond length of the studied molecule was 1.283(2) Å, which conforms that the double bond character exists between carbon and nitrogen atoms (Fig. 1, left). This bond length is almost same with the calculated value (1.289 Å). The mentioned dithiocarbazate group adopts an E-configuration relatively to the double bond between carbon-nitrogen atoms. The C11−S1 bond length of thione tautomeric form of studied molecule was 1.670(15) Å. Besides, the entire species has coplanar atoms with the exception of the S-benzyl phenyl ring, which is indicating that an electron delocalization occurs within the molecule. This bond length value of C11−S1 was found to be 1.654 Å as theoretically. The β-nitrogen and the thioketo sulfur were showed trans configuration due to the C11−N2 bond. The obtained value of bond length revealed that the C11−N2 bond was existed as single bond in the molecule and is in good agreement with the calculated value. Moreover, the values of bond length and bond angle of the studied compound showed that nitrogen and aromatic carbon atoms in the molecule have sp^2 hybrid character (Table 1).

3.4. Electrostatic results and mulliken electronegativity

The electron donating and receiving ability of a molecule can be defined using the value of HOMO and LUMO energy. These molecular orbitals play vital role in electronic and optical properties, luminescence, photochemical reaction, UV-VIS, quantum chemistry and pharmaceutical studies as well as provide the information of biological mechanism [45–49]. The frontier molecular orbital's (i.e., FMO's) energy gap supports to indicate the stability of structure. Besides, FMO's also informs about the kinetic stability and chemical reactivity of a molecule. Furthermore, the FMO's helps for predicting the most reactive position of a studied molecule. The calculated energy value of HOMO and LUMO orbitals are −0.26751 and −0.18094 eV, respectively. The FMO's energy gap (ΔE_{HOMO-}

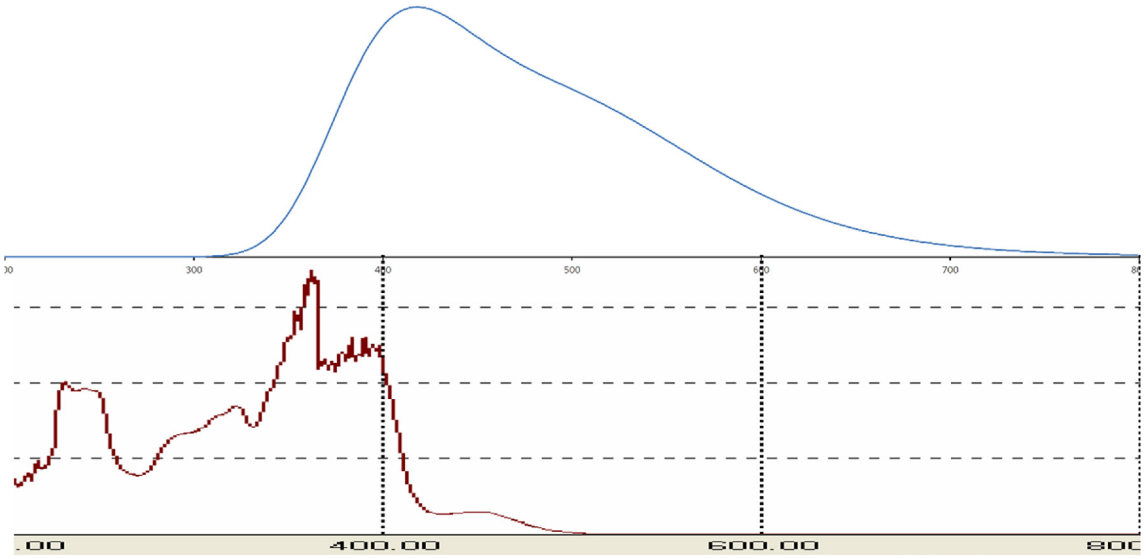

Fig. 3. Theoretical (up) and experimental (down) UV-VIS spectrum of compound **1**.

Table 1
Selected bond length (Å) and bond angle (°) for compound **1**.

Geometrical Parameters	Calculated	Observed	Geometrical Parameters	Calculated	Observed
C1–C2	1.389	1.371(3)	C1–C6	1.409	1.410(3)
C2–C3	1.416	1.409(3)	C3–C4	1.395	1.381(3)
C4–C5	1.399	1.395(3)	C5–C6	1.411	1.398(2)
C6–C10	1.457	1.456(2)	C12–C13	1.507	1.511(3)
C13–C14	1.404	1.386(3)	C13–C18	1.402	1.385(3)
C14–C15	1.396	1.385(3)	C15–C16	1.398	1.365(3)
C16–C17	1.397	1.371(3)	C17–C18	1.397	1.395(3)
C11–N2	1.362	1.336(2)	C10–N1	1.289	1.283(2)
C11–S2–C12	103.39	101.37(8)	C13–C14–C15	120.51	121.37(18)
N2–N1–C10	116.06	115.49(13)	C13–C18–C17	120.78	120.34(16)
C2–C1–C6	121.82	121.66(15)	N1–N2–C11	123.09	120.33(13)
O2–C3–C2	117.21	115.40(15)	O2–C3–C4	122.71	124.33(15)
C4–C5–C6	119.65	120.56(14)	C5–C6–C10	120.36	121.48(13)
C1–C6–C10	120.80	120.31(14)	S1–C11–S2	126.75	124.50(9)
S1–C11–N2	125.52	121.50(12)	S2–C11–N2	107.71	113.99(11)

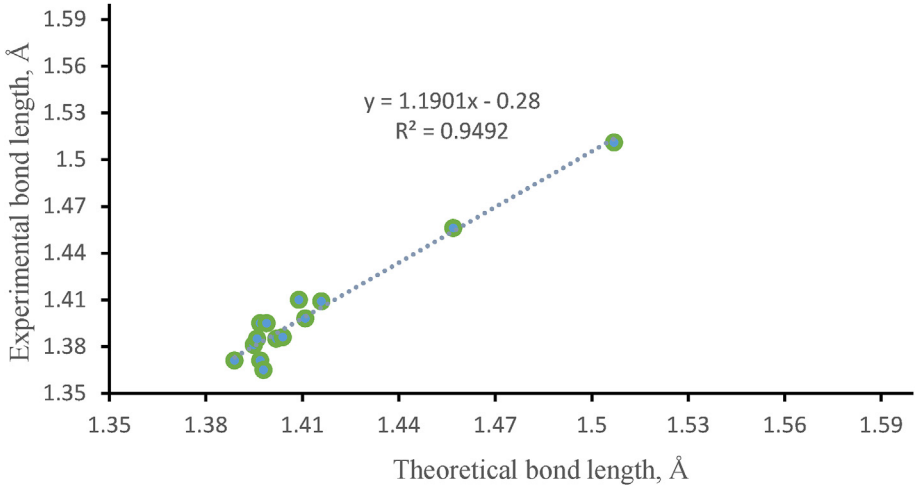

Fig. 4. Correlation diagram of bond length for compound **1**.

LUMO) of the mentioned organic molecule was found to be −0.08657 eV. The lower value of HOMO and LUMO energy gap showed that the studied molecule has high chemical reactivity, biological activity and polarizability. The frontier molecular orbital

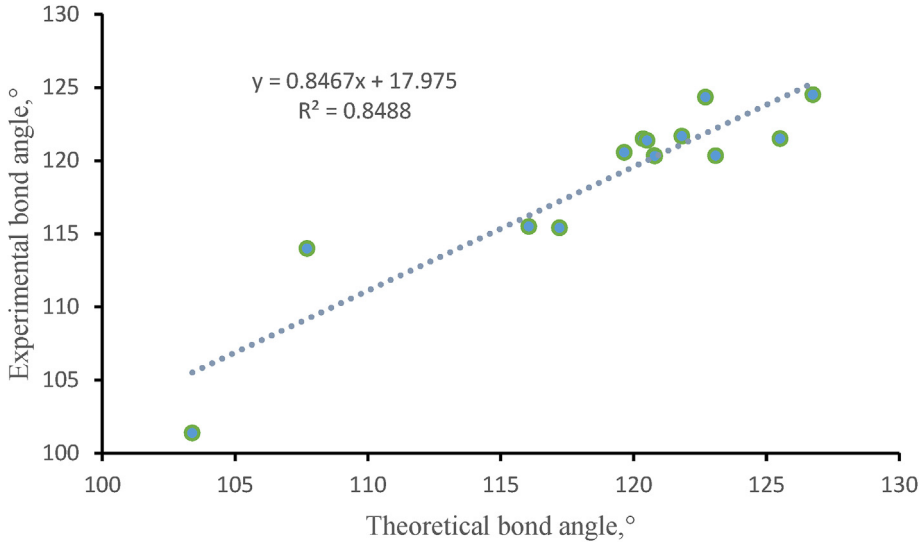

Fig. 5. Correlation diagram of bond angle for compound **1**.

distribution of the compound was depicted in Fig. 6. Moreover, the chemical reactivity parameters of the studied molecule such as chemical softness (S), chemical potential (μ), electrophilicity index (ω) and chemical hardness (η) were also carried out with the help of energy of HOMO and LUMO orbitals. The calculated value of chemical hardness, chemical potential as well as electrophilicity index and chemical softness for studied molecule was found to have 0.04, −0.22, 0.58 eV and 11.55 eV^{-1}, respectively. Electrophilicity index of a molecule informs about the binding ability of a compound with biomolecules [44,50,51]. The higher value of electrophilicity index of mentioned molecule showed that it has higher binding capacity with biomolecules and can act as an electrophilic species. While, the lower value of chemical hardness with high negative value of chemical potential means that the studied molecule is a soft molecule with high polarizibility. Futhermore, HOMO orbitals have mostly localized on sulfur atom, S15 and partially located on nitrogen atom (N13), azomethine group and methoxy group attached benzene ring (Fig. 6). While, LUMO orbitals were located on the whole molecule, but mostly located near the sulfur atom, S15, nitrogen atom (N13), azomethine group and methoxy group attached benzene ring.

3.5. Mulliken population analysis

Mulliken atomic charges of the optimized crystal structure were carried out by B3LYP/6-31+G(d,p) method in gas phase. The distribution of Mulliken atomic charge is tabulated in Table 2. The Mulliken atomic charges on carbon atoms were exhibited either positive or negative value. All hydrogen atoms were displayed a net positive charge, but H16 was gained maximum positive charge than the other hydrogen atoms, due to the presence of electronegative atom (N13). They act as acceptor atoms. Besides, all oxygen atoms of the optimized compound were shown to have negative charge, which act as donor atoms.

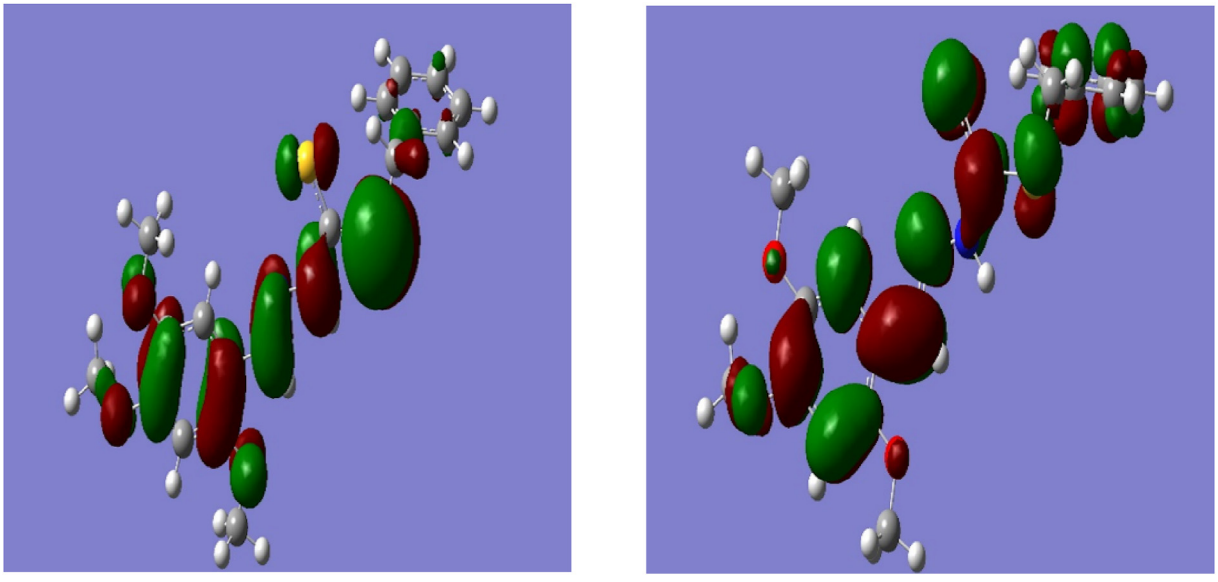

Fig. 6. HOMO (left) and LUMO (right) plot of compound **1.**

Table 2
Mulliken atomic charge of compound **1**.

Atom	Charge	Atom	Charge	Atom	Charge	Atom	Charge	Atom	Charge
C1	0.725301	C10	−0.903603	H19	0.119749	H28	0.129170	H37	0.153549
C2	0.593998	C11	−0.776762	C20	−0.103310	H29	0.127625	H38	0.111691
C3	−0.554817	N12	0.295406	C21	−0.223107	H30	0.119679	H39	0.150903
C4	0.127749	N13	−0.279076	C22	0.851136	H31	0.180698	C40	−0.141155
C5	0.245151	S14	0.077841	C23	−0.397223	H32	0.128447	H41	0.129807
C6	−1.243883	S15	0.598803	C24	−0.368889	H33	0.130925	H42	0.148212
H7	0.167735	H16	0.305065	C25	−0.114700	O34	−0.360772	H43	0.155347
H8	0.123178	H17	0.247872	H26	0.127846	C35	−0.200583	O44	−0.359263
C9	−0.068235	H18	0.219145	H27	0.118413	C36	−0.128638	O45	−0.386424

3.6. Molecular electrostatic potential surface

The molecular electrostatic potential (MEP) uses to predict the relative reactivity positions in a species for nucleophilic and electrophilic attack. The MEP surface analysis of the compound was determined by the DFT calculation using the optimized structure with B3LYP/6-31G+(d,p) basis set. The electrostatic potential surface mapped of the studied compound is given in Fig. 7. The color code of the compound lies in the range of $-4.618e^{-3}$ to $+4.618e^{-3}$. Red and blue color in the MEP structure point to more electron rich and electron poor region respectively.

The polarization effect is clearly seen in the compound. In the MEP, the negative potential regions are localized over the electronegative atoms (oxygen, nitrogen and sulfur) and the positive potential regions are localized over the hydrogen atoms. But sulfur atom of the compound is less negative potential site than the other electronegative atoms. Therefore, the more negative electronegative potential and positive electrostatic potential sites are more favorable for the attraction of nucleophilic and electrophilic species.

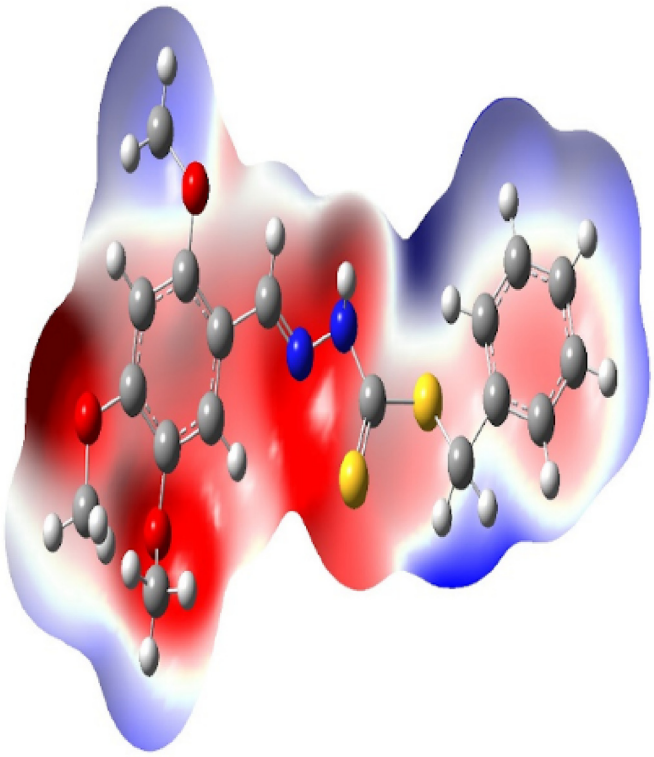

Fig. 7. Molecular electrostatic potential of compound **1.**

3.7. Harmonic oscillator model of aromaticity index

The aromaticity term is frequently used in organic chemistry. The aromaticity of homocyclic and heterocyclic compounds can be evaluated by harmonic oscillator model of aromaticity (HOMA) [52–54]. In order to calculate the geometrical aromaticity of homocyclic molecule, we have split the HOMA index into GEO and EN destabilizing terms. Both terms lead to decrease of the value of HOMA. Therefore, the HOMA can be written as follows:

$$\mathrm{HOMA} = 1 - \frac{1}{n}\sum_i \alpha\left(R_{opt} - R_i\right)^2 = 1 - \mathrm{EN} - \mathrm{GEO}$$

Where

$$\mathrm{GEO} = \frac{1}{n}\sum_i \alpha(R_{av} - R_i)^2$$

and

$$\mathrm{EN} = \alpha\left(R_{opt} - R_{av}\right)^2$$

The HOMA index value is close to 1 for the purely aromatic, close to 0 value for non-aromatic species [52–54]. The experimental value of GEO, EN and HOMA of the mentioned molecule were found to have 0.1363, 0.0093 and 0.9394 for C1–C6 ring and 0.0060, 0.0120 and 0.9618 for C13–C18 ring. On the other hand, in theoretically these values were found to be 0.0517, 0.0593 and 0.9173 for C1–C6 ring and 0.0064, 0.0318 and 0.9666 for C13–C18 ring. The theoretical and experimental results indicated that the both rings are the aromatic in nature.

3.8. Natural population analysis

The natural population analysis (NPA) of an organic compound reveals the distribution of electrons in various sub shells in atomic orbitals. The natural energies on individual atom and the accumulation of electron in the core, valance and Rydberg sub-shells are tabulated in Table 3. The value of natural charges informs that the atoms O45 was showed more electronegativity than O34 and O44 atoms. On the other hand, the N13 atom was gained more electronegative charge than N12 atom. Whereas, the atoms C3, C4 and C6 contain nearly same positive charge. H17 and H18 atoms were also gained more electropositive charge.

According to electrostatic point of view, more electronegative atom can easily donate their electron and most electropositive atom can accept an electron. The electrons of the mentioned compound were concentrated on the sub-shell as follows:

Core: 65.97790 (99.9665% of 66)
Valence: 131.35649 (99.5125% of 132)
Rydberg: 0.66560 (0.3362% of 198)

Table 3
Summary of natural population analysis of compound **1**.

Atom No.	Natural charge (e)	Natural population (e)			
		Core	Valence	Rydberg	Total (e)
C1	−0.14243	1.99891	4.12601	0.01752	6.14243
C2	−0.20691	1.99898	4.19253	0.01540	6.20691
C3	0.21469	1.99861	3.76383	0.02288	5.78531
C4	0.28834	1.99859	3.68962	0.02345	5.71166
C5	−0.32943	1.99895	4.31687	0.01362	6.32943
C6	0.32425	1.99864	3.65638	0.02073	5.67575
H7	0.27932	0.00000	0.71791	0.00277	0.72068
H8	0.25659	0.00000	0.74122	0.00218	0.74341
C9	0.04943	1.99932	3.92698	0.02427	5.95057
C10	−0.27447	1.99937	4.23101	0.04409	6.27447
C11	−1.06682	1.99891	5.02861	0.03930	7.06682
N12	−0.26530	1.99933	5.23798	0.02799	7.26530
N13	−0.50850	1.99943	5.47646	0.03260	7.50850
S14	0.04997	9.99861	5.91317	0.03825	15.95003
S15	0.61515	9.99867	5.30958	0.07661	15.38485
H16	0.40072	0.00000	0.59368	0.00560	0.59928
H17	0.43773	0.00000	0.55762	0.00465	0.56227
H18	0.42450	0.00000	0.57075	0.00475	0.57550
H19	0.20953	0.00000	0.78695	0.00352	0.79047
C20	−0.21347	1.99918	4.19867	0.01561	6.21347
C21	−0.26397	1.99902	4.25012	0.01484	6.26397
C22	−0.02879	1.99881	4.00601	0.02397	6.02879
C23	−0.35937	1.99888	4.33515	0.02534	6.35937
C24	−0.19030	1.99912	4.17413	0.01706	6.19030
C25	−0.26963	1.99917	4.25437	0.01610	6.26963
H26	0.24854	0.00000	0.75008	0.00138	0.75146
H27	0.24081	0.00000	0.75748	0.00171	0.75919
H28	0.28390	0.00000	0.71161	0.00449	0.71610
H29	0.24696	0.00000	0.75148	0.00156	0.75304
H30	0.24326	0.00000	0.75509	0.00165	0.75674
H31	0.25683	0.00000	0.73986	0.00331	0.74317
H32	0.18665	0.00000	0.81099	0.00235	0.81335
H33	0.22355	0.00000	0.77519	0.00126	0.77645
O34	−0.53919	1.99978	6.52109	0.01831	8.53919
C35	−0.33509	1.99928	4.31581	0.01999	6.33509
C36	−0.34260	1.99933	4.32889	0.01439	6.34260
H37	0.22327	0.00000	0.77509	0.00164	0.77673
H38	0.20057	0.00000	0.79699	0.00244	0.79943
H39	0.23020	0.00000	0.76865	0.00115	0.76980
C40	−0.32019	1.99945	4.30599	0.01475	6.32019
H41	0.20131	0.00000	0.79680	0.00189	0.79869
H42	0.23277	0.00000	0.76627	0.00096	0.76723
H43	0.21470	0.00000	0.78308	0.00221	0.78530
O44	−0.55019	1.99978	6.53288	0.01753	8.55019
O45	−0.57689	1.99979	6.55756	0.01954	8.57689

3.9. Natural bond orbital

The natural bond orbital investigation gives the information of conjugative interaction, hyper-conjugative interaction, intra and inter-molecular hydrogen bonding in a compound [48,55–57]. The natural bond orbital calculation was performed using NBO method [58,59] under Gaussian 09W program package at B3LYP method with 6-31G+(d,p) basis set. For each donor NBO (i) and acceptor NBO (j), the donor-acceptor stabilization energy E(2) associated with $i \rightarrow j$ delocalization is calculated as

$$E(2) = q_i . F(i,j)^2/(\varepsilon_j - \varepsilon_i)$$

where q_i is the donor orbital occupancy (2 for closed-shell, 1 for open-shell), ε_i, ε_j are diagonal elements (orbital energies) and F(i,j) is the off-diagonal NBO Fock matrix element [55,60,61]. The whole molecular system enjoys the greater extent of conjugation owing to the larger value of the stabilization energy, E2. Thus, the electron delocalization between occupied Lewis and unoccupied non-Lewis type natural bond orbitals can stabilize the donor-acceptor interaction. The electron density of conjugated single and double bond of the conjugated system clearly indicates more delocalization within the molecular system. From the output results of NBO analysis, the total Lewis structure has 97.42% (core, 99.97% and valance Lewis 96.14%) and non-Lewis structure has 2.58% (valance non-Lewis, 2.36% and Rydberg non-Lewis, 0.22%) in the studied compound. The various type of interactions, such as $\pi \rightarrow \pi^*$, $\sigma \rightarrow \pi^*$, $n \rightarrow \pi^*$, $n \rightarrow \sigma^*$, $\pi^* \rightarrow \pi^*$ and $\sigma \rightarrow \sigma^*$ were appeared in the theoretical result (Table 4), while only $\pi \rightarrow \pi^*$ and $n \rightarrow \pi^*$ interactions were observed in electronic spectral analysis as expected. Thus, the NBO results revealed that the calculated above two transitions are in good agreement with the observed electronic spectrum. The obtained results from NBO analysis showed that the σ(C1–C2) bond was formed from the $sp^{1.80}$ hybrid orbital on carbon (64.21% p-character) interacting with a $sp^{1.92}$ hybrid on carbon (65.67% p-character) in NBO analysis (Table 4). The $sp^{3.13}$ hybrid on carbon atom was interacted with a $sp^{2.68}$ hybrid of oxygen atom for the formation of σ(C3–O45) bond. The $sp^{2.06}$ hybrid orbital of carbon (67.29% p-character) was interacted with $sp^{1.37}$ hybrid on nitrogen (57.69% p-charcter) and formed σ(C9–N12) bond. For the formation of σ(C10–S14) bond, the $sp^{1.63}$ hybrid orbital of carbon (61.90% p-character) was interacted with $sp^{3.24}$ hybrid on sulfur (75.89% p-character) atom.

The π(C–C) interactions and antibonding π*(C–C) interactions are most responsible for the conjugation of respective π* bonds in aromatic rings. The interactions πC1-C2 to π*C3–C4 and π*C5–C6; πC3-C4 to π*C1–C2 and π*C5–C6 and πC5-C6 to π*C1–C2 and π*C3–C4 were observed in the C1/C6 benzene ring containing stabilization energy of 18.02, 24.04; 21.81, 16.42 and 16.58, 21.91 kcal/mol, respectively (Table 5). Similarly, in the case of C20/C25 benzene ring, the interactions πC20-C21 to π*C22–C23 and π*C24–C25; πC22-C23 to π*C20–C21 and π*C24–C25 and πC24-C25 to π*C20–C21 and π*C22–C23 were found to be 21.35, 16.81; 16.32, 19.51 and 22.96, 18.16 kcal/mol, respectively. The aforementioned stabilization energies are more responsible for the stability of the benzene rings and for the intramolecular charge transfer of the studied compound. The energies for the interaction n_2O34 to π*C3–C4 and n_2O44 to π*C5–C6 were 19.03 and 18.55 kcal/mol, respectively. The aforesaid energies were stabilized the structure of studied molecule and proved the resonance

Table 4
Occupancy of natural orbitals and hybrids of compound **1** for C, H, O, N, S atoms.

Parameters	Occupancies (e)	Hybrids	Atomic orbitals (%)
σC1 - C2	1.96744	$sp^{1.80}$	s(35.76%)p(64.21%)d(0.04%)
σC1 – C9	1.97053	$sp^{2.38}$	s(29.57%)p(70.39%)d(0.03%)
σC3 - O45	1.98794	$sp^{3.13}$	s(24.17%)p(75.63%)d(0.20%)
σC9 - N12	1.98947	$sp^{2.06}$	s(32.61%)p(67.29%)d(0.10%)
σC9 - H19	1.98704	$sp^{1.95}$	s(33.88%)p(66.07%)d(0.05%)
σC10 - S14	1.99052	$sp^{1.63}$	s(37.98%)p(61.90%)d(0.11%)
σN12 - N13	1.98163	$sp^{3.28}$	s(23.35%)p(76.51%)d(0.14%)
σN13 - H16	1.96849	$sp^{3.15}$	s(24.05%)p(75.88%)d(0.06%)
σC22 - C23	1.96531	$sp^{1.77}$	s(36.09%)p(63.86%)d(0.05%)
nN12	1.92521	$sp^{1.89}$	s(34.56%)p(65.37%)d(0.07%)
nS14	1.97919	$sp^{0.30}$	s(77.00%)p(22.96%)d(0.04%)
nS15	1.92992	$sp^{0.48}$	s(67.65%)p(32.33%)d(0.02%)
nO34	1.97022	$sp^{1.30}$	s(43.49%)p(56.46%)d(0.05%)
nO44	1.96652	$sp^{1.25}$	s(44.41%)p(55.54%)d(0.05%)
nO45	1.94686	$sp^{1.30}$	s(43.49%)p(56.44%)d(0.07%)
σ*C1 – C2	0.01735	$sp^{1.80}$	s(35.76%)p(64.21%)d(0.04%)
σ*C1 – C9	0.03026	$sp^{2.38}$	s(29.57%)p(70.39%)d(0.03%)
σ*C3 – O45	0.02937	$sp^{3.13}$	s(24.17%)p(75.63%)d(0.20%)
σ*C9 – N12	0.00782	$sp^{2.06}$	s(32.61%)p(67.29%)d(0.10%)
σ*C9 – H19	0.02785	$sp^{1.95}$	s(33.88%)p(66.07%)d(0.05%)
σ*C10 – S14	0.03266	$sp^{1.63}$	s(37.98%)p(61.90%)d(0.11%)
σ*N12 – N13	0.02094	$sp^{3.28}$	s(23.35%)p(76.51%)d(0.14%)
σ*N13 – H16	0.02726	$sp^{3.15}$	s(24.05%)p(75.88%)d(0.06%)
σ*C22 – C23	0.03274	$sp^{1.77}$	s(36.09%)p(63.86%)d(0.05%)

Table 5
Second-order perturbation analysis of the interaction between donor and acceptor orbitals of compound **1** in NBO basis.

Donor (i)	Type	Acceptor (j)	Type	E(2), kcal/mol	Donor (i)	Type	Acceptor (j)	Type	E(2), kcal/mol
C1−C2	σ	C1−C6	σ*	3.43	N12−N13	σ	C1−C9	σ*	2.78
		C1−C9	σ*	1.26			C10−C14	π*	0.81
		C2−C3	σ*	2.09	C20−C21	π	C22−C23	π*	21.35
		C2−H7	σ*	1.36			C24−C25	π*	16.81
C1−C2	π	C5−C6	π*	24.04	C20−C25	σ	C20−C21	σ*	2.12
		C3−C4	π *	18.02			C24−C25	σ*	2.04
C1−C6	σ	C5−C6	σ*	2.91	C22−C23	σ	C23−C24	σ*	3.86
C1−C9	σ	C9−N12	σ*	1.09	C22−C23	π	C20−C21	π*	16.32
		N12−N13	σ*	5.21			C24−C25	π*	19.51
C2−C3	σ	C1−C2	σ*	2.33	C23−C24	σ	C22−C23	σ*	3.98
		C4−O34	σ*	3.79			C23−H28	σ*	1.72
C3−C4	σ	C4−C5	σ*	2.90			C24−H29	σ*	0.91
		C36−O45	σ*	0.72	C24−C25	σ	C20−C25	σ*	2.03
C3−C4	π	C1−C2	π*	21.81			C23−C24	σ*	2.38
		C5−C6	π *	16.42	C24−C25	π	C20−C21	π*	22.96
C4−C5	σ	C3−C4	σ*	3.18			C22−C23	π*	18.16
		C3−O45	σ*	4.06	N12	n_1	C1−C9	σ*	2.55
		C5−H8	σ*	1.66	N13	n_1	C9−N12	σ*	0.62
C5−C6	σ	C1−C6	σ*	3.54			C10−S15	σ*	1.70
		C1−C9	σ*	3.37	S14	n_1	C10−N13	σ*	2.99
C5−C6	π	C1−C2	π*	16.58			C10−S15	σ*	3.28
		C3−C4	π*	21.91	S15	n_1	C10−S14	σ*	4.16
C9−N12	σ	C10−N13	σ*	1.62		n_2	C10−S14	π*	25.70
C9−N12	π	C1−C2	π*	5.48	O34	n_1	C3−C4	σ*	5.07
		C9−N12	π*	0.54		n_2	C3−C4	π*	19.03
C10−N13	σ	C11−S15	σ*	0.75	O44	n_1	C5−C6	σ*	5.15
C10−S14	σ	N13−H16	σ*	0.58		n_2	C5−C6	π*	18.55
C10−S14	π	C10−S14	π*	0.86	O45	n_1	C3−C4	σ*	1.98
C11−S15	σ	C11−C22	σ*	0.64		n_2	C2−C3	σ*	6.16
		C21−C22	σ*	8.13	C3−C4	π*	C1−C2	π*	270.05
C20−C21	σ	C20−C25	σ*	2.02	C5−C6	π*	C1−C2	π*	255.00
		C20−H26	σ*	0.99	C9−N12	π*	C1−C2	π*	103.13
		C21−C22	σ*	3.23	C22−C23	π*	C20−C21	π*	173.98
		C21−H27	σ*	1.33			C24−C25	π*	130.97

interaction occurs between hetero atoms and aromatic ring. Therefore, the whole system of the compound enjoys greater extent of conjugation. The donor orbital n_2S14 was also exhibited strongest interaction having higher stabilization energy (18.48 kcal/mol), which supports in favor of intra-molecular hydrogen bond between S14 atom and N13−H16 (N13−H16 …. S14). Additionally, the highest stabilization energy (Table 4) containing π*C3−C4 → π*C1−C2, π*C5−C6 → π*C1−C2, π*C9−N12 → π*C1−C2, π*C22−C23 → π*C20−C21 and π*C24−C25 interactions clearly lead to intermolecular charge transfer process in the studied molecule. Additionally, the intramolecular charge transfer and redistribution of electron in various orbitals within the compound were occurred, which is clearly ensured by NBO and simulated electronic spectral analysis.

3.10. Molecular docking investigation

Molecular docking is an essential technique in structure-based drug design and can be used in facilitating and speeding up the development of drugs. Molecular docking informs scientists to virtually screen of the interaction between the ligand and target protein as well as predicts the binding conformations and affinities of any species to target protein. The recent emergence of the novel coronavirus threatens public health across the world and World Health Organization declares this as global pandemic. But the specific drug treatment against covid-19 are yet to be discovered. Thus, in order to search new drug, we have performed *in silico* evaluation of the compound within the active site of coronavirus to explore how it interact. A greater negative value of binding energy of any species reveals that it has the better docking ability to target protein as well as the docking of ligand and target protein were selected based on the related binding energy value. The inhibition constant (K_i) of the studied species was calculated from the binding energy (ΔG) with the help of $K_i = \exp(\Delta G/RT)$ equation, where R is the universal gas constant (1.987×10^{-3} kcal mol^{-1} K^{-1}) and T is the temperature (298.15 K). The calculated binding energy of the compound **1,** azithromycin and hydroxychloroquine with target protein was found to be −6.0, −7.3 and −5.6 kcal/mol, respectively. While, the calculated inhibition constant values of the aforesaid species were 39.54, 4.45 and 77.73 μM, respectively. The obtained results revealed that the binding energy of the compound **1** is higher than that of hydroxychloroquine and slightly lower than that of azithromycin. Besides, the inhibition constant values also indicated that the compound **1** has higher ability to inhibit the biological process of target protein than hydroxychloroquine. Generally, the ligand binds with docking sites of target protein through various interactions such as hydrogen bond, hydrophobic bond and electrostatic bond type interactions. These types of interactions were appeared in molecular docking simulation of the studied compounds. From the docking cavity, it was seen that CYS145, GLU166, GLN189 and HIS163 amino acids of target protein were interacted with the studied compound **1**, in which SH group of CYS145 was formed hydrogen bond interaction with oxygen of methoxy group of compound **1** and the bonding distance was 3.54 Å (Fig. 8). Besides, carbonyl group of GLU166, GLN189 and HIS163 amino acids was also formed hydrogen bond by the interaction with hydrogen of methoxy group of compound **1** with bond distance 1.87, 3.78 and 3.73 Å, respectively. Furthermore, carbonyl group of GLU166 was also showed an electrostatic interaction with nitrogen of NH group of compound **1**. While, PRO168 and HIS41 amino acids were docked with pi-electron of benzene ring of compound **1** through hydrophobic interactions. The bonding

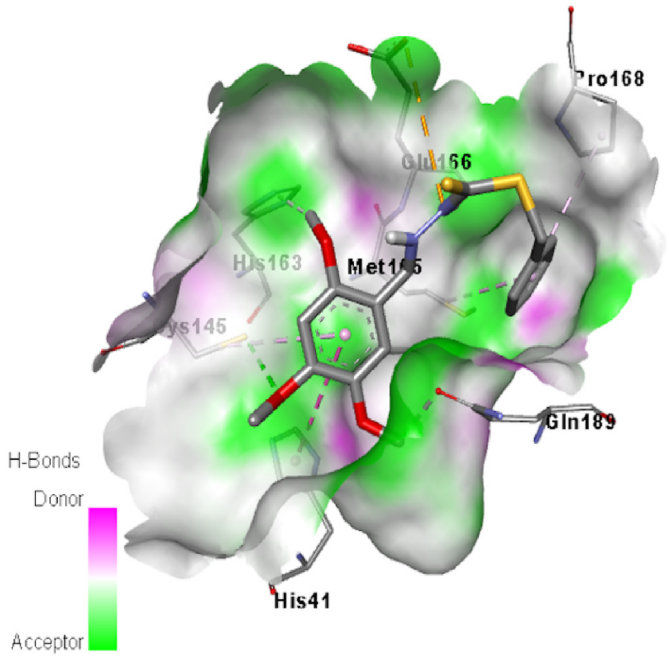

Fig. 8. Binding modes of compound **1**, with target protein.

distances were 5.40 and 5.50 Å, respectively. Another hydrophobic interaction was seen in the docking site, which was formed by the interaction of pi-electron of benzene of compound **1** and sulfur of MET165 amino acid residue. The obtained docking results revealed that the drug component, azithromycin was formed two hydrogen bonds with THR199 and LEU287 amino acids (Fig. 9, left). The bonding distance of first hydrogen bond was found to be 3.18 Å, while the distance of second hydrogen bond was 3.70 Å. Besides, three hydrophobic interactions were identified between azithromycin and MET276, TRY239 and TRY237 amino acids residues in docking sites. The distances of three hydrophobic interactions were found to be 3.88, 4.94 and 4.51 Å. For the case of hydroxychloroquine, it was showed first hydrogen bond interaction between NH of GLN192 and the oxygen of hydroxyl group of hydroxychloroquine (Fig. 9, right). The bond distance was found to be 3.08 Å. Another hydrogen bond interaction was obtained between oxygen of carbonyl group of ARG188 and the hydrogen of hydroxyl group of hydroxychloroquine and the bond distance was 2.44 Å. The third hydrogen bond interaction was also being appeared between carbonyl group of Glu166 and NH of hydroxychloroquine compound and the bond distance was 3.62 Å. Moreover, three hydrophobic interactions were observed between PRO168, HIS41 and MET49 amino acid residues and hydroxychloroquine compound in the docking pose. The obtained bond distances were found to be 4.18, 4.96 and 4.82 Å, respectively.

3.11. Assessment of drug-likeness and ADMET analysis

Most of the leads cannot make their appearance to the market due to their poor absorption, distribution, metabolism, excretion and toxicity issues, which are generally known as ADMET. In this study, drug-likeness and ADMET of the compound **1** were investigated. The predicted results of the studied compound are tabulated in Table 6. The drug-likeness of a compound is assessed by Lipinski's rule of five (RO5) and Jorgensen's rule of three. Compound with a fewer or preferably no violations are likely to be considered as a potential drug candidate. The results showed that there was no violation of Lipinski's rule of five (RO5) and Jorgensen's rule of three, indicating the drug-likeness of the compound. The compound showed excellent absorption owing to its promising solubility, lipophilicity and permeability. The number of rotatable bond and polar surface area indicated high bioavailability of the studied compound. From the predicted value of QPloghERG, it has been found to be safe for drug-induced hERG (human ether-a-go-go-related gene) related cardiotoxicity, as hERG K+ channel blockers lead to QT interval prolongation and fatal cardiac arrhythmia. Moreover, the compound was found to be CNS inactive. The number of metabolites and other parameters were also within the permissible range. The toxicity profile of the studied compound was carried out using ProTox II. The designed compound has shown good toxicity profile based on toxicity risk assessment. The predicted LD_{50} value of the compound was 700 mg/kg, which belongs to toxicity class 4. The predicted results suggested that the compound was non-carcinogenic in nature and has no effect on immunotoxicity, mutagenicity and cytotoxicity.

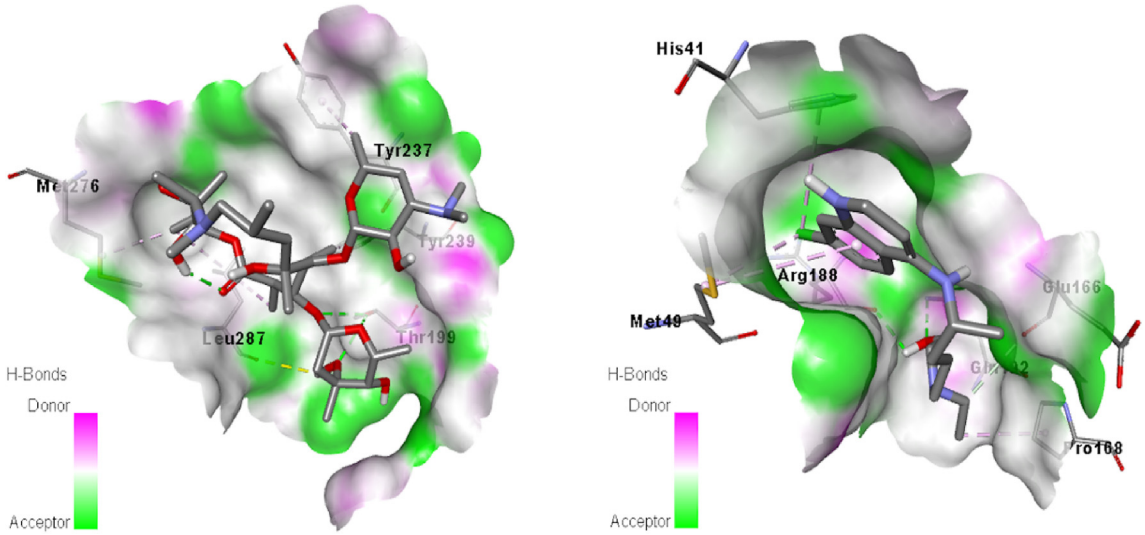

Fig. 9. Binding pose of azithromycin (left) and hydroxychloroquine (right) with target protein.

Table 6
Prediction of ADME properties of compound **1**.

Parameter	Observed value	Parameter	Observed value	Parameter	Observed value
HBD	1	QPlogS	−5.87	QPPCaco	4672.84
HBA	5.75	QPlogPw	8.725	QPPMDCK	7235.64
Molecular weight	376.48	QPlogPo/w	4.88	Human Oral Absorption	3
PSA	51.82	QPlogKhsa	0.396	% Human Oral Absorption	100
metab	4	QPlogBB	−0.16	CNS	0
#rotor	9	QPlogKp	−0.304	QPloghERG	−6.414

4. Conclusion

The most characteristic azomethine group of compound **1** showed a band at 1668 cm^{-1} as expected. The theoretical and experimental values of infrared and UV-VIS spectra for the studied compound were almost same. Bond lengths and bond angles obtained from crystal data were in excellent agreement with theoretical values. The molecular electrostatic potential of the studied compound showed suitable regions to attack for electrophilic and nucleophilic substances. The mentioned compound is highly chemically reactive and acts as a soft molecule. Both benzene rings of the compound were aromatic in character due to calculated HOMA value. The molecular docking analysis showed that the compound **1** has relatively more binding affinity with the target protein than hydroxychloroquine. Moreover, the compound followed all the parameters of Lipinski's rule of five. It also showed good ADME properties and toxicity profile that makes the compound a potential drug candidate and may be considered for further drug development.

Funding source

This work was not supported by any funding source.

Ethical approval

Not required.

CRediT authorship contribution statement

Mohammad Abdul Mumit: Conceptualization, Data curation. **Tarun Kumar Pal:** Formal analysis, Writing - original draft, Software, Supervision. **Md Ashraful Alam:** Methodology. **Md Al-Amin-Al-Azadul Islam:** Investigation. **Subrata Paul:** Writing - review & editing. **Md Chanmiya Sheikh:** Visualization.

Declaration of competing interest

The authors have no conflicts of interest to declare.

Appendix A. Supplementary data

Supplementary data to this article can be found online at https://doi.org/10.1016/j.molstruc.2020.128715.

References

[1] L.H. Abdel-rahman, A.M. Abu-dief, H. Moustafa, A.A.H. Abdel-mawgoud, Design and nonlinear optical properties (NLO) using DFT approach of new Cr(III), VO(II), and Ni(II) chelates incorporating tri-dentate imine ligand for DNA interaction , antimicrobial , anticancer activities and molecular docking studies, Arab. J. Chem. 13 (2020) 649–670.
[2] F.C. Lima, T.S. Silva, C.H.G. Martins, C.C. Gatto, Synthesis, crystal structures and antimicrobial activity of dimeric copper (II) complexes with 2-hydroxyphenyl-ethylidene-dithiocarbazates, Inorg. Chim. Acta. 483 (2018) 464–472.
[3] S.M. Abdallah, M.A. Zayed, G.G. Mohamed, Synthesis and spectroscopic characterization of new tetradentate Schiff base and its coordination compounds of NOON donor atoms and their antibacterial and antifungal activity, Arab. J. Chem. 3 (2010) 103–113.
[4] M.S. Begum, E. Zangrando, M.C. Sheikh, R. Miyatake, M.B.H. Howlader, M.N. Rahman, A. Ghosh, Bischelated complexes of a dithiocarbazate N,S Schiff base ligand: synthesis, characterization and antimicrobial activities, Transit. Met. Chem. (2017).
[5] M. Ghassemzadeh, F. Akhoundpour, S. Bahemmat, B. Neumuller, Synthesis , characterization , and molecular structure of a new dimeric silver (I) complex containing 1 , 2 , 4-triazole moiety, Monatsh. Chem. (2013) 2–6.
[6] F.N. How, K.A. Crouse, M.I.M. Tahir, M.T.H. Tarafder, A.R. Cowley, Synthesis, characterization and biological studies of S- benzyl- b - N - (benzoyl) dithiocarbazate and its metal complexes, Polyhedron 27 (2008) 3325–3329.
[7] A. Islam, C. Sheikh, M.A. Mumit, R. Miyatake, M.A. Alam, M.O.A. Mondal, Synthesis, characterization and antimicrobial activity of a bidentate NS Schiff base of S-benzyl dithiocarbazate and its divalent complexes, J. Coord. Chem. 69 (2016) 3580–3592.
[8] M. Khaled, M.I.M. Tahir, K.A. Crouse, T. Khoo, Synthesis, characterization , and bioactivity of Schiff bases and their Cd^{2+}, Zn^{2+}, $Cu2^{+}$, and Ni^{2+} complexes derived from chloroacetophenone isomers with S-benzyldithiocarbazate and the X-Ray crystal structure of S-Benzyl- β-N- (4-chlorophenyl)methylened, Bioinorgan. Chem. Appl. (2013) 1–13, 2013.
[9] A.I. Osman, Uwaisulqarni M. Zolkipli, Fatin Aliyah Daud, Synthesis, characterization and geometry optimization of benzyl 3-[(e, e)-3-phenylprop-2-enylidene]dithiocarbazate (BPED) via DFT studies, J Sustain Sci Manag (2017) 80–85, 2017.
[10] M. Cleiton, L. Daniel, L. V Modolo, R.B. Alves, M.A. De Resende, C.V.B. Martins, Schiff bases, A short review of their antimicrobial activities, J. Adv. Res. 2 (2011) 1–8.
[11] E. Hejchman, H. Kruszewska, D. Maciejewska, B. Sowirka, Młynarczuk-Biały, M. Tomczyk, A. Sztokfisz-Ignasiak, J. Jankowski, Design, synthesis and biological activity of Schiff bases bearing salicyl and 7 - hydroxycoumarinyl moieties, Monatsh. Chem. 150 (2019) 255–266.
[12] M.A. Malik, O.A. Dar, P. Gull, M.Y. Wani, A.A. Hashmi, Heterocyclic Schiff base transition metal complexes in antimicrobial and anticancer chemotherapy, Med. Chem. Commun. 9 (2017) 409–436.
[13] A. Kajal, S. Bala, S. Kamboj, N. Sharma, V. Saini, Schiff Bases : a versatile pharmacophore, J. Catal. 2013 (2013).
[14] M.H. Islam, M.C. Sheikh, M.A.A.A.A. Islam, Studies on coordination chemistry and antibacterial activity of bidentate NS Schiff base derived from SBDTC and 4-benzyloxybenzaldehyde, J. Sci. Res. 11 (2019) 121–132.
[15] B. Derkowska-zielinska, M. Barwiolek, C. Cassagne, G. Boudebs, Nonlinear optical study of Schiff bases using Z-scan technique, Optic Laser. Technol. 124 (2020) 105968.
[16] M. Vairalakshmi, R. Princess, B.K. Rani, S.J. Raja, Synthesis, structural elucidation, catalytic, antibacterial and antioxidant activity of thiophene derived mixed ligand metal complexes, J. Chil. Chem. Soc. 63 (2018) 3844–3849.
[17] I.P. Ejidike, P.A. Ajibade, Transition metal complexes of symmetrical and asymmetrical Schiff bases as antibacterial, antifungal, antioxidant and anticancer agents: progress and prospects, Rev. Inorg. Chem. 35 (2015) 191–224.
[18] M. Evecen, H. Tanak, Quantum chemical studies on the molecular structure, spectroscopic and electronic properties of (6-Methoxy-2-oxo-2H-chromen-4-yl)-methyl pyrrolidine-1-carbodithioate, Mater Sci-Poland 34 (2016) 886–904.
[19] H.F. Adly, M.I. Omima, El-shafiy, New metal complexes derived from S-benzyldithiocarbazate (SBDTC) and chromone-3- carboxaldehyde: synthesis, characterization, antimicrobial, antitumor activity and DFT calculations, J. Coord. Chem. 72 (2019) 218–238.
[20] M. Kumar, T. Padmini, K. Ponnuvel, Synthesis, characterization and antioxidant activities of Schiff bases are of cholesterol, J. Saudi Chem. Soc. 21 (2017) S322–S328.
[21] S.A. Aly, S.K. Fathalla, Preparation, characterization of some transition metal complexes of hydrazone derivatives and their antibacterial and antioxidant activities, Arab. J. Chem. 13 (2020) 3735–3750.
[22] I.P. Ejidike, P.A. Ajibade, Synthesis, characterization, anticancer and antioxidant studies of RU(III) complexes of monobasic tridentate Schiff bases, Bioinorgan. Chem. Appl. (2016) 1–11, 2016.
[23] H.F. Abd El-Halim, G.G. Mohamed, M.N. Anwar, Antimicrobial and anticancer activities of Schiff base ligand and its transition metal mixed ligand complexes with heterocyclic base, Appl. Organomet. Chem. 32 (2018) 1–12.

[24] R. Mudavath, R.K. Vuradi, U. Bathini, N. Narsimha, S. Kunche, S.N.T. Sunitha, S.D. Ch, Design, synthesis, in vitro anticancer, antioxidant and antibacterial activity; DNA/BSA binding, photoleavage and docking studies of Cu(II) ternary metal complexes, Nucleos Nucleot Nucl 38 (2019) 874–900.
[25] P. Hohenberg, W. Kohn, Inhomogeneous electron gas, Phys. Rev. 136 (1964) B864–B872.
[26] W. Kohn, L.J. Sham, Self-consistent equations including exchange and correlation effects, Phys. Rev. 140 (1965) A1133–A1138.
[27] R. Haunschild, A. Barth, B. French, A comprehensive analysis of the history of DFT based on the bibliometric method RPYS, J. Cheminf. 11 (2019) 1–15.
[28] X. Ma, D. Chang, C. Zhao, R. Li, X. Huang, Z. Zeng, X. Huang, Y. Jia, Geometric structures and electronic properties of the Bi2X2Y (X,Y=O, S, Se, and Te) ternary compound family: a systematic DFT study, J. Mater. Chem. 6 (2018) 13241–13249.
[29] S. Naseem, M. Khalid, M.N. Tahir, M.A. Halim, A.A.C. Braga, M.M. Naseer, Z. Shafiq, Synthesis, structural, DFT studies, docking and antibacterial activity of a xanthene based hydrazone ligand, J. Mol. Struct. 1143 (2017) 235–244.
[30] R.D. Dennington, T.A. Keith, J.M. Millam, Semichem, Inc., 2016.
[31] C. Lee, W. Yang, R.G. Parr, Phys. Rev. B 37 (1988) 785.
[32] M.J. Frisch, G.W. Trucks, H.B. Schlegel, G.E. Scuseria, M.A. Robb, J.R. Cheeseman, G. Scalmani, V. Barone, B. Mennucci, G.A. Petersson, H. Nakatsuji, M. Caricato, X. Li, H.P. Hratchian, A.F. Izmaylov, J. Bloino, G. Zheng, J.L. Sonnenberg, Gaussian, Inc., CT Wallingford, 2009.
[33] M. Katari, E. Nicol, V. Steinmetz, G. van der Rest, D. Carmichael, G. Frison, Improved infrared spectra prediction by DFT from a new experimental database, Chem. Eur J. 23 (2017) 8414–8423.
[34] S. Muthu, J. Uma Maheswari, Quantum mechanical study and spectroscopic (FT-IR, FT-Raman, 13C, 1H, UV) study, first order hyperpolarizability, NBO analysis, HOMO and LUMO analysis of 4-[(4-aminobenzene) sulfonyl] aniline by ab initio HF and density functional method, Spectrochim. Acta Mol. Biomol. Spectrosc. 92 (2012) 154–163.
[35] The PyMOL Molecular Graphics System, Version 2.0 Schrödinger, LLC.
[36] N.M. O'Boyle, M. Banck, C.A. James, C. Morley, T. Vandermeersch, G.R. Hutchison, Open Babel: an open chemical toolbox, J. Cheminf. 2 (2011) 297.
[37] Dassault Systemes BIOVIA, Discovery Studio Visualizer 4 (5) (2016), 2016.
[38] R. Singh, Synthesis , spectral studies and quantum-chemical investigations on S-benzyl b -N- (4-NN biscynodi ethylaminophenylmethylene) dithiocarbazate, Arab. J. Chem. 12 (2019) 1537–1544.
[39] N. Özdemir, R. Kąıt, O. Dayan, Investigation of enol-imine/keto-amine tautomerism in (E)-4-[(2-hydroxybenzylidene)amino]phenyl benzenesulphonate by experimental and molecular modelling methods, Mol. Phys. 114 (2016) 757–768.
[40] F. Cuenú, J. Londoño-salazar, J.E. Torres, R. Abonia, R.F.D. Vries, Synthesis, structural characterization and theoretical studies of a new Schiff base 4- (((3-(tert-Butyl)-(1-phenyl)pyrazol-5-yl) imino)methyl)phenol, J. Mol. Struct. (2017).
[41] I. Rama, R. Selvameena, Synthesis , structure analysis , anti-bacterial and in vitro anti-cancer activity of new Schiff base and its copper complex derived from sulfamethoxazole, J. Chem. Sci. 127 (2015) 671–678.
[42] M. Mesbah, T. Douadi, F. Sahli, S. Boukazoula, Synthesis , characterization , spectroscopic studies and antimicrobial activity of three new Schiff bases derived from Heterocyclic moiety, J. Mol. Struct. 1151 (2018) 41–48.
[43] C. Ali, Ru(III), Cr(III), Fe(III) complexes of Schiff base ligands bearing phenoxy Groups : application as catalysts in the synthesis of vitamin K3, J. Saudi Chem. Soc. 22 (2018) 757–766.
[44] S. Alyar, S. Tülin, Synthesis , spectroscopic characterizations , enzyme inhibition , molecular docking study and DFT calculations of new Schiff bases of sulfa drugs, J. Mol. Struct. 1185 (2019) 416–424.
[45] H. Ebrahimi, J.S. Hadi, H.S. Al-Ansari, A new series of Schiff bases derived from sulfa drugs and indole-3-carboxaldehyde: synthesis, characterization, spectral and DFT computational studies, J. Mol. Struct. 1039 (2013) 37–45.
[46] S.A. Beyramabadi, Fluorescence and DFT studies (molecular structure , IR and NMR spectral assignments , NBO and Fukui function) of Schiff bases derived from 2-chloro-3-quinolinecarboxaldehyde, J. Struct. Chem. 59 (2018) 1392–1402.
[47] H.P. Ebrahimi, J.S. Hadi, A.A. Almayah, Z. Bolandnazar, A.G. Swadi, A. Ebrahimi, Metal-based Biologically Active Azoles and β-lactams Derived from Sulfa Drugs, Elsevier Ltd, 2016.
[48] Z. Demircioğlu, Ç.A. Kaştaş, O. Büyükgüngör, The spectroscopic (FT-IR, UV-vis), fukui function, NLO, NBO, NPA and tautomerism effect analysis of (E)-2-[(2-hydroxy-6-methoxybenzyli- dene)amino]benzonitrile, Spectrochim. Acta Mol. Biomol. Spectrosc. 139 (2015) 539–548.
[49] S. Kumar, V. Saini, I.K. Maurya, J. Sindhu, M. Kumari, R. Kataria, V. Kumar, Design , synthesis , DFT , docking studies and ADME prediction of some new coumarinyl linked pyrazolylthiazoles : potential standalone or adjuvant antimicrobial agents, PloS One 13 (2018) 1–23.
[50] S. Mondal, S.M. Mandal, T.K. Mondal, C. Sinha, Structural characterization of new Schiff bases of sulfamethoxazole and sulfathiazole, their antibacterial activity and docking computation with DHPS protein structure, Spectrochim. Acta Mol. Biomol. Spectrosc. 150 (2015) 268–279.
[51] G. Banuppriya, R. Sribalan, V. Padmini, Synthesis and characterization of curcumin-sulfonamide hybrids : biological evaluation and molecular docking studies, J. Mol. Struct. 1155 (2018) 90–100.
[52] C.P. Frizzo, M.A.P. Martins, Aromaticity in heterocycles: new HOMA index parametrization, Struct. Chem. 23 (2012) 375–380.
[53] I. Majerz, T. Dziembowska, Aromaticity of benzene derivatives: an exploration of the cambridge structural database, Acta Crystallogr. B 74 (2018) 148–151.
[54] A. Kanaani, D. Ajloo, G. Grivani, A. Ghavami, M. Vakili, Tautomeric stability, molecular structure, NBO, electronic and NMR analyses of salicylideneiminpo-ethylimino-pentan-2-one, J. Mol. Struct. 1112 (2016) 87–96.
[55] R.P. Gangadharan, Natural bond orbital (NBO) population analysis of 1-Azanapthalene-8-ol, Acta Phys. Pol., A 125 (2014) 18–22.
[56] D.M. Suresh, M. Amalanathan, S. Sebastian, D. Sajan, I.H. Joe, V.B. Jothy, I. Nemec, Vibrational spectral investigation and natural bond orbital analysis of pharmaceutical compound 7-Amino-2,4-dimethylquinolinium formate–DFT approach, Spectrochim. Acta Mol. Biomol. Spectrosc. 115 (2013) 595–602.
[57] K. Science, E. Journal, X-ray and DFT Investigation of (E)-4-bromo-5-methoxy-2-((o-tolylimino) methyl) phenol Compound, Karaelmas Sci. Eng. J. 8 (2018) 454–461.
[58] A.J. Foster, F. Weinhold, Natural hybrid orbitals, J. Am. Chem. Soc. 102 (1980) 7211–7218.
[59] E.D. Glendening, J.K. Badenhoop, A.E. Reed, J.E. Carpenter, J.A. Bohmann, C.M. Morales, C.R. Landis, F. Weinhold, NBO Version 3.1, Tci, University of Wisconsin, Madison, 1998, p. 65.
[60] R. Bhuvaneswari, M.D. Bharathi, G. Anbalagan, G. Chakkaravarthi, K.S. Murugesan, Molecular structure, vibrational spectroscopic (FT-IR, FT-Raman), NBO, HOMO and LUMO analysis of morpholinium oxalate by density functional method, J. Mol. Struct. 1173 (2018) 188–195.
[61] A. Khalil, S. Abdel, A. Kh, TD-DFT calculations , NBO analysis and electronic absorption spectra of some thiazolo [3, 2-a] pyridine derivatives TD-DFT calculations , NBO analysis and electronic absorption spectra of some thiazolo [3, 2-a] pyridine derivatives, J. Mol. Struct. 1147 (2017) 651–667.